Using fiber bragg gratings for shape monitoring and adjustment of a thermal protection system aboard a targeted re-entry cubesat

Vanhamel , J.; Eaton, Nicholas; Spreij, Roemer

Publication date
2022

Document Version
Final published version

Citation (APA)
Vanhamel , J., Eaton, N., & Spreij, R. (2022). *Using fiber bragg gratings for shape monitoring and adjustment of a thermal protection system aboard a targeted re-entry cubesat*. Paper presented at The 2nd International Conference on Flight Vehicles, Aerothermodynamics and Re-entry Missions Engineering (FAR), Heilbronn, Germany.

USING FIBRE BRAGG GRATINGS FOR SHAPE MONITORING AND ADJUSTMENT OF A THERMAL PROTECTION SYSTEM ABOARD A TARGETED RE-ENTRY CUBESAT

Jurgen Vanhamel(1)(2), Nicholas Eaton(3) and Roemer Spreij(4)

(1) Technical University of Delft (TU Delft), Faculty of Aerospace Engineering, Section Space Systems Engineering, Kluyverweg 1, 2629 HS Delft, The Netherlands
(2) KU Leuven, Electronic Circuits and Systems, Kleinhoefstraat 4, 2440 Geel, Belgium
(3) Space Acoustics GmbH, Peterwise 3, 8197 Rafz, Switzerland
(4) Von Karman Institute, Waterloosesteenweg 72, 1640 Sint-Genesius-Rode, Belgium

ABSTRACT

Currently, the amount of space debris is increasing rapidly due to the tremendous amount of satellite launches. Having an autonomous re-entry system aboard satellites at their end-of life, creates possibilities in the frame of lowering space debris, as well as for sample return from space. This paper aims at describing two possible deployment systems for the Thermal Protection System. Also, the integration of an onboard Fibre Bragg Grating-based shape monitoring system, coupled to an adaptive control system is described. Additionally, several re-entry trajectory steering systems are investigated, combined with an inflatable concept analysis. The combination of a deployable Thermal Protection System, an onboard closed feedback loop for shape monitoring, and the ability to adapt the shape of the Thermal Protection System, creates the possibility to design an autonomous dynamically steered re-entry system.

Index Terms— Thermal Protection System, cubesat, Fibre Bragg Grating, shape monitoring, heat shield

1. INTRODUCTION

The life time of satellites in orbit is limited, i.c. from a few months up to several years. At end-of-life, these vehicles have to be removed from their functional orbit. This can be done by actively putting them in a graveyard orbit, or by active/passive re-entry into the atmosphere. The latter can cause issues related to atmospheric contamination [1]. If this re-entry is done in an uncontrolled manner, an additional risk exists related to over-land impact [2] which may cause human casualties.

The awareness of debris in space, as well as the removal of dysfunctional satellites and other objects is put high on the agenda. Several techniques are under development to mitigate space debris [3, 4, 5]. Especially for cubesats, no targeted full recovery re-entry system exists. If such a system is fully operational, this would impose an advantage from a pollution point-of-view: a full recovery of the spacecraft and payload prevents the release of harmful substances into the atmosphere, which is not the case with traditional space debris removal techniques. The risk of human casualties should at least meet the European Code of Conduct for Space Debris Mitigation, stating re-entry casualty risk has to be below 1 to 10,000 [6]. If this re-entry is done in a controlled manner, this requirement can also be fulfilled.

Additionally, if a targeted full recovery re-entry system is implemented aboard a cubesat, this opens the possibility of sample return from space. If, for example, a cubesat with a sample return container and a dedicated Thermal Protection System (TPS) are developed, a more flexible transportation system can be put in place for sample return from the ISS and for other sample return setups. A Nanoracks CubeSat Deployer (NRCSD) facility is already available aboard the ISS [7], hence this does not involve any additional cost. The cubesat design, containing a TPS, should fit the requirements imposed by the cubesat launch facility.

Interests in re-entry systems has increased in recent years. Several deployable systems have been under investigation [8, 9]. A potential sample return mission faces three main challenges: 1) offering protection from the high temperatures during re-entry, 2) steering the cubesat during re-entry in order to follow a predefined trajectory, and 3) safely landing the cubesat after passing through the atmosphere. The aim of this paper is to propose an initial idea on the first two points.

2. TPS DESIGN

In order to offer protection from the high temperatures during re-entry, compared to a traditional, fixed-geometry TPS, inflatable or deployable structures offer high drag with a low impact on the mass, greatly lowering the ballistic coefficient.

The deceleration during re-entry occurs at a high altitude, and with low heat fluxes [10]. This lowers the demand on the TPS and benefits sample return missions, which may have stringent requirements on the temperature of the payload. Such systems have long been considered for ISS return

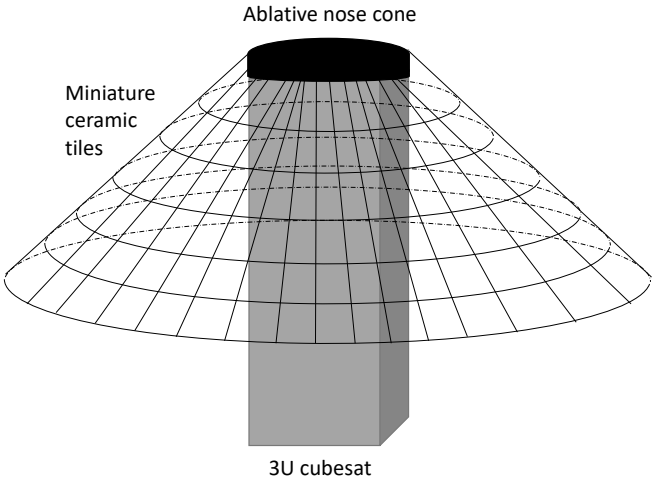

Fig. 1. Possible TPS setup: ablative nose cone, combined with flexible miniature temperature resistant ceramic tiles.

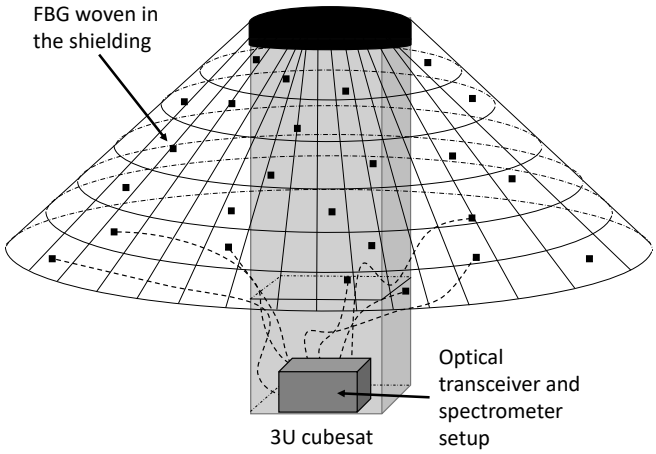

Fig. 2. The FBGs are equally distributed inside the TPS, combined with the optical transceiver and spectrometer inside a 1U, together with the other onboard systems (not all FBG connections to the transceiver and spectrometer are indicated in the figure).

missions and Mars entries, with existing development so far limited to large-scale devices such as the Inflatable Re-entry and Descent Technology (IRDT) and Inflatable Re-entry Vehicle Experiment (IRVE) missions [11, 12]. A fixed-geometry TPS uses ablative material or temperature resistant ceramic tiles, whereas the developed TPS would have a dynamically controlled flexible shape. The latter can be a combination of an ablative structure on top of the cubesat, with flexible miniature temperature resistant ceramic tiles [13] integrated in a deployed TPS (Fig. 1).

The system to deploy the TPS can be inflatable or mechanical. A trade-off has to be performed which approach is most suitable to be housed inside a 10 x 10 x 10 cm cube (= 1U cubesat dimension).

2.1. Inflatable TPS

The inflatable TPSs that have been tested or are under development use conical TPS shapes, which are a proven, aerodynamically stable design. If an inflatable system is used, a dedicated inflation system should be selected, able to initiate and maintain pressure. For this, e.g. nitrogen can be used housed inside a small container [14], or gas generators can be applied. This system of course will consume a significant amount of volume and mass aboard the cubesat. Subsequently, the complexity of the TPS increases. This needs further study.

2.2. Mechanical deployable TPS

For the mechanical deployment system, already designs are developed using a rib and strut structure, combined with a rigid nose on top of the TPS [9]. The idea would be to design a mechanical deployable system, small enough to be housed inside a 1U. An in-depth study is necessary to investigate the deployment system, using springs or other unfolding mechanisms.

A trade-off is necessary between the size of the TPS and the exposed temperature range, the used material, as well as an analysis of the feasibility of both described deployment concepts.

3. TPS SHAPE MONITORING

In order to steer the cubesat during re-entry, a monitoring system using Fibre Bragg Gratings (FBGs) is developed, implemented inside the TPS. A distributed fibre network, combined with an optical transceiver and a spectrometer (Fig. 2), is able to measure at certain points directly the mechanical and thermal stresses inside the shield, by encoding the strain at their position into an optical wavelength. Each measurement node is connected to a transceiver and spectrometer as indicated in Figure 2 (not all connections of the nodes are shown). This setup can be developed by using compact sized, high sampling frequency measurement opto-electronics, in which a time division multiplexed approach for multiple sensors and multiple channels is applied. This enables the measurement of the strain fields and the dynamic stresses inside the TPS. The exact amount, distribution and placing of the measurement nodes is under investigation. This also depends on the used optical transceiver and spectrometer available for space applications.

For embedding FBGs in Bismaleimide (BMI) / woven glass composite, additional insulation is expected for the hottest

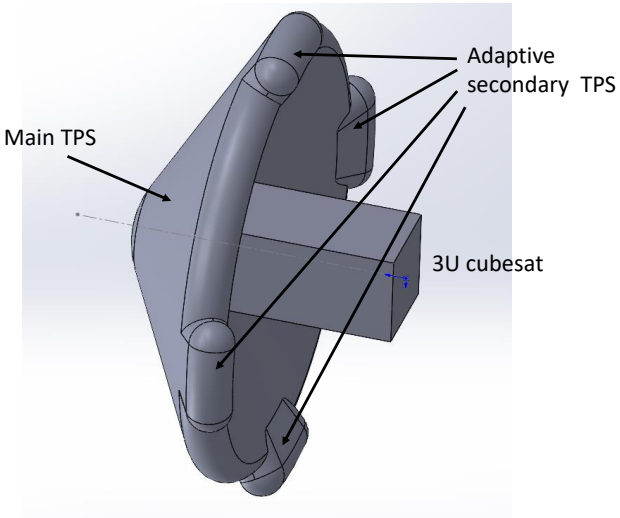

Fig. 3. A double inflatable TPS approach, able to adjust the re-entry trajectory, based on an onboard feedback system, using the FBGs.

area of the heat shield, around the shock zone forming ahead of the shield center. Various types of optical fibre sensors have been explored. The FBG type has advantages in this application because of the localized strain measurement and small sensor size. In general, the materials and FBG sensors for a flexible, high strength shield operating up to 250°C are already well developed [15]. An extended material tradeoff analysis will be necessary, including cork/phenolic, silicone, etc., supported by transient thermal analyses methods.

Previous work by the team has shown that standard 125 micron diameter optical fibre with low sensitivity to bending and a thin (10 micron range) polyimide coating can be embedded reliably in a wide range of woven and unidirectional fibre reinforced composite laminates. They can be operated successfully between -196°C and +250°C, with repeated stress and temperature cycles. This research demonstrated that 80-60 micron diameter optical fibres are feasible and are advantageous for the compact and highly curved flexible heat shield.

This setup allows a translation into a model which can give a view on the shape of the inflatable TPS during the re-entry process. For the deployable TPS, the FBGs shall be distributed equally on the ribs and struts in order to monitor the deployment status of the structure. Additionally, the FBG network shall be woven-into the TPS material itself. Hence, also the status of the deployed TPS can be monitored. This allows a real-time shape analysis of the TPS, for which the information is analyzed in the onboard computer system.

4. RE-ENTRY TRAJECTORY STEERING SYSTEMS

The following section details some trajectory adjustment concepts using inflatable, deployable and Shape Memory Alloy (SMA) actuation methods. To gauge the capabilities of the inflatable concept, a 6 Degrees Of Freedom (DOF) trajectory simulation is performed in section 5, along with a preliminary stability analysis.

4.1. Trajectory adjustment using an inflatable system

Trajectory control using an offset Centre Of Gravity (COG) along with bank angle control to direct the lift vector, is a proven concept. It is used for human capsules (Apollo, Soyuz) and Mars landers such as MSL [16], as well as during the Inflatable Re-entry Vehicle Experiment 3 (IRVE-3) mission [17]. Dillman et al. [18] note that this guidance strategy results in a coupling of the Angle of Attack (AoA) and sideslip angles, as well as the downrange and crossrange error at landing. Fuel expenditure limits the number of bank angle reversals and adds weight. Instead, they propose Direct Force Control (DFC) for an inflatable system as an alternative method where the AoA and sideslip are controlled separately. Either by means of four rigid flaps on the outer diameter of the TPS, or by straps pulling on the TPS from the center body of the spacecraft. The inflatable system considered in this section is similar to the flap concept, but uses four secondary inflatable bellows at the rim of the primary, conical inflatable TPS (Fig. 3). By inflating or deflating these smaller bellows, using a dedicated inflation system, a dynamic steering during re-entry can be achieved.
Using the above described DFC approach, in combination with the described onboard FBG closed loop feedback system for TPS shape monitoring (section 3), opens the opportunity to monitor and adapt the re-entry trajectory in real-time.

4.2. Trajectory adjustment using a deployable system

An adaptive TPS for re-entry vehicles was already described by A. Fedele et al. [19]. They use multiple steerable metal flap structures, which are put in the slipstream in order to steer the vehicle during re-entry. If a deployable TPS is used instead of an inflatable one, the idea described by A. Fedele et al. [19] could be combined with the FBGs closed-loop feedback monitoring setup, in order to have an alternative full autonomous re-entry system.

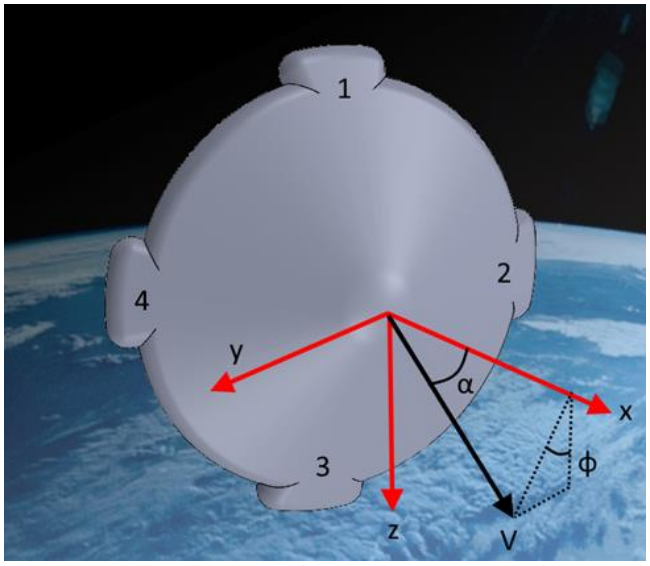

Fig. 4. 3U cubesat with deployed flaps, showing body axes definition and numbering of flaps.

Velocity [m/s]	7800
Flight path angle [°]	-1
Altitude [km]	120

Table 1. Trajectory simulation initial conditions.

Deployed flaps	Case name	Case designation
None	0	0
3	1, up	1U
1	1, down	1D
4	1, left	1L
2	1, right	1R
3, 4	2, up & left	2UL
2, 3	2, up & right	2UR
1, 4	2, down & left	2DL
1, 2	2, down & right	2DR
2, 3, 4	3, up	3U
1, 2, 4	3, down	3D
1, 3, 4	3, left	3L
1, 2, 3	3, right	3R
1, 2, 3, 4	4	4

Table 2. Flaps configurations.

4.3. Trajectory adjustment using SMA

Another idea can be the use of SMA to adapt a deployable TPS [20]. The major advantage of this technique, is the 'memory effect' this metal has. The metal has the ability of returning to its original shape if heat is applied. The use of SMA in the field of aerospace applications, is already described [21]. In these applications morphing structures are used, e.g. for flap camber control in the aviation industry [22]. In this approach, the structural shape of certain material is adapted, by applying a certain amount of heat. By varying the temperature, the shape of the metal can be varied. Depending on the used SMA material, a different temperature range needs to be applied [23]. The high temperature ranges for SMAs can cause issues in low-power cubesat applications. Hence, dedicated SMA material has to be examined, especially for the TPS application. Also, external heating from the re-entry can affect the SMA operation and has to be taken into account in the design.
Nitinol Nickel-Titanium SMA is well developed and already applied in space applications in actuators for mechanism deployment [24]. Wires with diameters in the range of 25 – 500 microns are readily available with actuation force capabilities in the 0.3 to 110 N range. The displacement range is about 4 %, the actuation time about 3 seconds. Direct resistance heating of the wire is possible. Potential difficulties are the temperature isolation of the wires from the background and the high current needed. A potential solution is to package the SMA wires inside insulating silicone tubes. Shape control approach can be effected by integrating the wires radially about the shield as reinforcing straps, and varying their length between actuated and non-actuated values by electrical heating of the wires. SMA actuators can be used to deploy the inflatable heat-shield in the form of gas control valves, hold-down and release latches.

All three systems described above, create the ability of automatically adapt and control the re-entry trajectory of the cubesat. Hence, a safe and targeted re-entry can be aimed at. The future idea is to integrate these systems into a 1U setup, which can be implemented as an additional payload aboard any cubesat.

5. INFLATABLE CONCEPT ANALYSIS

5.1. Simulation parameters

The system considered here is shown in Figure 4. It consists of a 3U cubesat with a 60 degree half-angle conical TPS. The nose radius is 10 cm and the TPS diameter is 50 cm. Four tubular inflatable bellows or 'flaps' are added at the rim with equal spacing. They each extend another 30 mm beyond the outer diameter, and are 30 degrees wide. This analysis is intended to estimate the performance of the system by looking at the extreme trajectories: those where one or more of the bellows is inflated completely. This will give an outer limit to the achievable landing range. Degrees of flap deployment between zero and full deployment are not considered, and the design of a control system to reach any location within this outer landing range is left to a later study.

Trajectory calculations were made using ROVT (Royal Observatory – VKI Trajectory code, in-house developed), a

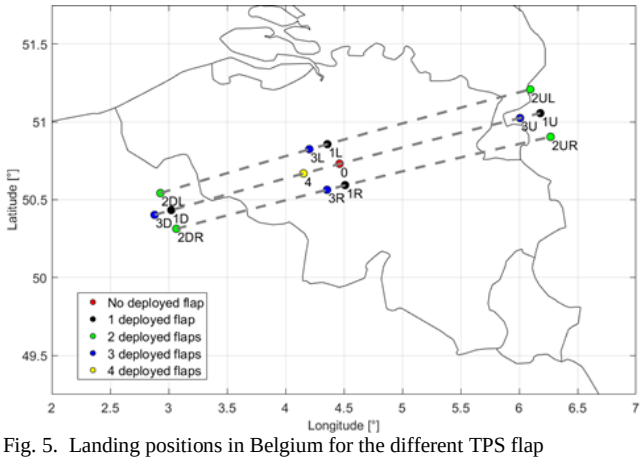

Fig. 5. Landing positions in Belgium for the different TPS flap configurations.

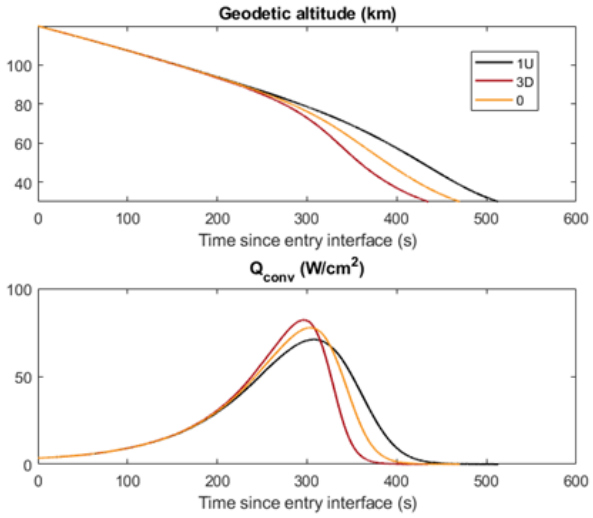

Fig. 6. Heat flux and altitude vs. time for the 1U, 3D and 0 (no flaps) configuration.

simulator developed by the Von Karman Institute (VKI) and the Royal Observatory of Belgium. Starting from an initial state (Table 1), 6DOF trajectories are propagated for five configurations of the TPS: with zero, one, two, three or all four bellows inflated. The initial state was chosen to correspond with a typical entry after a decaying orbit (something that can be expected from an unpowered cubesat), with a hypothetical landing area over Belgium. The initial attitude of the cubesat is with its flaps aligned with the local horizontal (flaps 2-4) and vertical (flaps 1-3) directions. For the configurations with one, two and three inflated flaps, four cases are simulated with different choices of flaps. Table 2 lists the cases and naming, according to the direction the satellite is steered in. The remaining two possible configurations with two deployed flaps opposite each other is not considered.

Aerodynamic coefficients for each configuration were calculated using ANTARES (Application of Newtonian Theory for ARbitrary Entry Shapes), a VKI-developed tool [25]. ANTARES is a panel method that uses modified Newtonian Theory applicable for hypersonic continuum flight. The aerodynamic coefficients are as follows:

$$C_{F,i}(\alpha,\varphi) = \frac{F_i}{\frac{1}{2}q\,S} \quad (1)$$

$$C_{M,i}(\alpha,\varphi) = \frac{M_i}{\frac{1}{2}q\,S_{ref}\,L_{ref}} \quad (2)$$

F_i and M_i are the forces and moments corresponding to the different axes, q is the dynamic pressure, and S_{ref} and L_{ref} are a reference surface and length, taken to be the TPS frontal projected area and diameter. The simulation ends when 30 km altitude is reached, at which point the assumptions underlying ANTARES break down (hypersonic flight, or approximately M > 5).

Case	Peak heat flux [MW/m^2]
1U	0.71
0	0.77
3D	0.82

Table 3. Peak heat fluxes.

5.2. Simulation results

Figure 5 shows the 'landing locations' (position at the end of the simulation, at 30 km altitude) for each simulation, overlaid with great circle sections. The length of the landing zone is 243.4 km, and the width is 31.1 km, for a total landing zone area of 7569.74 km². The area is symmetric in the cross-track direction, but asymmetric along-track, with the 1U case landing 147.1 km further than case 0 and the 3D case 130.4 km before it.

Looking at heat flux, Figure 6 shows the convective heat flux for configurations 1U, 0 and 3D (the first and last being the most extreme cases) computed with the correlation by Sutton-Graves [26]:

$$q = k\sqrt{\frac{\rho}{R}}V^3 \quad (3)$$

Where ρ is the density, R the nose radius, V the velocity and k atmosphere dependent constant (k = 1.7415e-4 kg$^{1/2}$m^{-1} for Earth). The peak heat fluxes are listed in Table 3.

5.3. Conclusion

The simulations performed show that an appreciable degree of control over the final landing location can be achieved with deployable flaps placed around an inflatable TPS. The ultimate range around a central landing point has a footprint of 7569.74 km^2. For contrast, the Utah Test and Training Range, used in the past as landing area for deep space entry missions Stardust and Genesis [27, 28], has an area of 6930 km^2. The central landing point could be set by a dedicated deorbit burn or conceivably, drag-based deorbiting techniques as implemented in the TechEdSat cubesat series [29]. This last concept could also use the inflatable TPS and its flaps as means of controlling the drag, combined with the FBG monitoring system. The simulations also show that independent control over the in-track and cross-track errors is possible with this design. For example, compare cases 1U and 2UL: the addition of flap 3 to the 1U configuration only affects the cross-track landing position, without affecting the in-track position. This is the advantage of DFC. Concerning the heat flux, the concept offers a reduced peak heat flux of 0.71 to 0.82 MW/m^2 compared to a non-deployable heat shield design: the QARMAN re-entry satellite, built at VKI and launched in 2019, experienced expected heat fluxes of 1.7 MW/m^2 during its entry in February 2022 [30] (simulated values, contact with QARMAN was lost before entry and no data was gathered from the flight). QARMAN used an 1U ablative cork heatshield at the nose of the vehicle, along with solar panels deployed in a dart configuration for aerodynamic stability.

5. CONCLUSION AND FURTHER WORK

The use of a real-time onboard steerable deployable or inflatable TPSs, opens the possibility of having a fully controlled re-entry cubesat. The idea is to develop a TPS, made of specific material, which can withstand the harsh environment of space during re-entry.

A trajectory analysis of a first concept, using an inflatable TPS with controllable secondary inflatable flaps, was done. With this design, a landing point inside a 243.4 by 31.1 km area can be reached, with a reduced heat flux compared to a traditional ablative shield.

The ability of having a dynamic steerable system integrated into the TPS, using an onboard FBG-based real-time feedback system, was explained. This will create possibilities, useful for the future exploration of space, as well as for full recovery of spacecrafts in the frame of minimizing space debris. The aim is to have a 1U size TPS, which can be integrated as a payload into the satellite.

Future work consist in performing a trade-off to select the most suitable TPS system. Subsequently, the selection of appropriate material for the deployable or inflatable TPS has to be done. Based on this trade-off, the FBGs have to be integrated into the TPS itself. For this, a dedicated distributed FBG network has to be developed, including the optical transceiver and spectrometer, coupled to the onboard computer system in order to design a real-time feedback setup. The latter can be used to steer the cubesat in a dynamic way using a secondary TPS, adaptive flaps or SMA, aiming at an autonomous controlled re-entry. Further detailed analysis like described in section 5, is needed. Also the design and implementation of a recovery system, in order to reach a specific location on ground after the re-entry, is part of future work.

6. REFERENCES

[1] L.S. Ivlev, K.Ya. Kondrat'ev, and S.N. Khvorostovskii, "The effect of space debris on the composition, optical properties, and physical processes in the upper and middle atmosphere," *J. Opt. Technol.*, vol. 68, no. 7, p. 457, 2001.

[2] E. Bergamini, et al., "The Increasing Risk of Space Debris Impact on Earth: Case Studies, Potential Damages, International Liability Framework and Management Systems," *Enhancing CBRNE Safety & Security: Proceedings of the SICC 2017 Conference*, Springer International Publishing, Cham, pp. 271–280, 2018.

[3] A. Viquerat, M. Schenk, B. Sanders, and V. J. Lappas, "Inflatable Rigidisable Mast For End-Of-Life Deorbiting System," *European Conference on Spacecraft Structures, Materials and Environmental Testing (SSMET)*, Braunschweig, Germany, April pp. 1–4, 2014.

[4] K.A. Monogarov, et al., "Uncontrolled Re-Entry of Satellite Parts after Finishing Their Mission in LEO: Titanium Alloy Degradation by Thermite Reaction Energy," *Acta Astronautica*, vol. 135, pp. 69–75, 2017.

[5] M.M. Castronuovo, "Active Space Debris Removal—A Preliminary Mission Analysis and Design," *Acta Astronautica*, vol. 69, no. 9, pp. 848–859, 2011.

[6] EU, "European Code of Conduct for Space Debris Mitigation", 28.06.2004. [Online]. Available: https://www.unoosa.org/documents/pdf/spacelaw/sd/2004-B5-10.pdf, Accessed on: Mar. 18, 2022.

[7] Nanoracks, Nanoracks CubeSat Deployer. [Online]. Available: https://nanoracks.com/products/iss-launch/, Accessed on : Mar. 18, 2022.

[8] T. Stone, et al., “SOAREX-8 Suborbital Experiments 2015 - A New Paradigm for Small Spacecraft Communication,” *2015 IEEE Aerospace Conference*, vol. 2015, pp. 1–7, 2015.

[9] A.M. Cassell, et al., “ADEPT, A Mechanically Deployable Re-Entry Vehicle System, Enabling Interplanetary CubeSat and Small Satellite Missions,” *32nd Annual AIAA/USU Small Satellite Conference*, vol. XII-08, 2015.

[10] R.T. Kendall and A.R. Maddox, “The Use of Inflatable Structures for Re-Entry of Orbiting Vehicles,” *SAE Technical Paper*, Warrendale, PA: SAE International, Sep. 1, 1990.

[11] L. Marraffa et al., “Inflatable Re-Entry Technologies: Flight Demonstration and Future Prospects”, *ESA Bulletin*, August 2000.

[12] D. Litton et al., “Inflatable Re-Entry Vehicle Experiment (IRVE) - 4 Overview”, *21st AIAA Aerodynamic Decelerator Systems Technology Conference and Seminar, Aerodynamic Decelerator Systems Technology Conferences*, American Institute of Aeronautics and Astronautics, 2011.

[13] A. Mühlratzer, et al. “Development of a New Cost-Effective Ceramic Composite for Re-Entry Heat Shield Applications,” *Acta Astronautica*, vol. 42, no. 9, pp. 533–540, 1998.

[14] L. Marraffa, et al. “Inflatable Re-Entry Technologies: Flight Demonstration and Future Prospects,” *E.S.A. Bulletin*, no. 103, pp. 78–85, 2000.

[15] N. Eaton, "Monitoring Dynamic Response of Composite Sandwich Panels Using New Optical Fibre Sensor Approach," *Proceedings of the 1st International Conference on Composites Dynamics (DYNACOMP)*, Arcachon, France, 2012.

[16] R. Prakash, et al. “Mars Science Laboratory Entry, Descent, and Landing System Overview,” *2008 IEEE Aerospace Conference*, pp. 1–18, 2008.

[17] R.A. Dillman, et al. “Attitude Control Performance of IRVE-3,” Conference paper, *(Preprint) AAS 13-077*, NASA Langley Research Center, 2014.

[18] R.A. Dillman, et al., “Low Lift-to-Drag Morphing Shape Design,” *AIAA Scitech 2020 Forum*, American Institute of Aeronautics and Astronautics, 2020.

[19] A. Fedele, et al. “Aerodynamic Control System for a Deployable Re-Entry Capsule,” *Acta Astronautica*, vol. 181, pp. 707–716, 2021.

[20] T.W. Duerig, *Engineering Aspects of Shape Memory Alloys*, Butterworth-Heinemann, 1990.

[21] L. Concilio, *Shape Memory Alloy Engineering: for Aerospace, Structural and Biomedical Applications*. 1st ed., Butterworth-Heinemann, 2015.

[22] B. Cees, et al. “Wing Morphing Control with Shape Memory Alloy Actuators,” *Journal of Intelligent Material Systems and Structures*, vol. 24, no. 7, pp. 879–898, 2013.

[23] J. Van Humbeeck, “Shape Memory Alloys: A Material and a Technology,” *Advanced Engineering Materials*, vol. 3, no. 11, pp. 837–850, 2001.

[24] G. Costanza, and M.E. Tata. “Shape Memory Alloys for Aerospace, Recent Developments, and New Applications: A Short Review,” *Materials*, vol. 13, no. 8, p. 1856, 2020.

[25] T. Durbin, G. Grossir, and O. Chazot, ‘Hypersonic Aerodynamic Predictions for Arbitrary Geometries Using ANTARES’, *HiSST: 2nd International Conference on High-Speed Vehicle Science & Technology*. Work submitted for publication (conference September 2022).

[26] K. Sutton, and R.A. Graves, “A general stagnation-point convective heating equation for arbitrary gas mixtures,” *NASA Technical Report*, Langley Research Center, 1971.

[27] P. N. Desai and G. D. Qualls, “Stardust Entry Reconstruction,” *Journal of Spacecraft and Rockets*, vol. 47, no. 5, pp. 736–740 , Sept. 2010.

[28] P. N. Desai, G. D. Qualls, and M. Schoenenberger, “Reconstruction of the Genesis Entry,” *Journal of Spacecraft and Rockets*, vol. 45, no. 1, pp. 33-38, Jan. 2008.

[29] K. Williams, “NASA’s Exo-Brake 'Parachute' to Enable Safe Return for Small Spacecraft,” August 7, 2017 [Online]. Available: https://www.nasa.gov/directorates/spacetech/small_spacecraft/feature/exo-brake_parachute, Accessed on : May. 22, 2022.

[30] I. Sakraker, “Aerothermodynamics of Pre-Flight and In-Flight Testing Methodologies for Atmospheric Entry Probes,” Ph.D. dissertation, VKI and Université de Liège, Belgium, 2016.